n-Alkane Homogeneous Nucleation: Crossover to Polymer Behavior

H. Kraack,[†] M. Deutsch,[†] and E. B. Sirota*[,‡]

Physics Department, Bar Ilan University, Ramat Gan, Israel, and ExxonMobil Research and Engineering Co., Corporate Strategic Research, Route 22 East, Annandale, New Jersey 08801

Received February 22, 2000; Revised Manuscript Received June 7, 2000

ABSTRACT: Homogeneous nucleation of crystallizing *n*-alkanes ($CH_3-(CH_2)_{n-2}-CH_3$, $17 \le n \le 60$) and some low-MW polyethylene (PE) fractions were studied using calorimetry and compared to reanalyzed PE data of Ross and Frolen. The undercooling and derived surface energy of the *n*-alkanes starts increasing for *n* as low as 25, far below the low-*n* limit for chain-folding. This behavior appears to extrapolate to the high undercooling exhibited by high-MW PE. The behavior is discussed in terms of a possible crossover between full-molecule nuclei of low-*n* and "bundle" nuclei of larger *n*. It is also related to the negentropic model, in that the surface energy increases when the "cilia" dangling from the bundle nucleus exceed a length where their entropic cost begins to significantly raise the surface energy. At low *n*, homogeneous nucleation occurs into the metastable rotator phase whose potential importance at high *n* is discussed.

Introduction

Both polyethylene (PE) and paraffin wax are made up of saturated linear hydrocarbon chains $CH_3-(CH_2)_{n-2}-CH_3$ (abbreviated C*n*). Paraffin waxes typically contain *n*-alkanes in the approximate range of $17 \le n \le 40$ while polyethylene has $n \gg 200$. The similarities in their crystallization are obvious: Crystallization is driven by the free energy of ordering the methylene sequences into the all-trans configuration and packing into an orthorhombic herringbone subcell structure. The differences occur at a longer length scale: The shorter *n*-alkane waxes order in crystalline layers whose spacing corresponds to the average molecular length and where the methyl groups lie at the interlamellar planes. Polyethylene usually forms crystals which are only a fraction of a molecular length thick and whose surface is populated by chain folds.[1] Under certain conditions, however, extended chain crystals form, where a crystal may be longer than an extended molecule, and no layering is present.[2] Chain folding sets in at $n \sim 200$ and has been reported to occur under certain crystallization conditions (i.e., very high-MW *n*-alkanes) for *n* as low as 150[3] and 120.[4] On the other hand, extended chain pure *n*-alkane crystals cannot form (at atmospheric pressure) for *n* above 550.[5]

The kinetic aspects of PE and wax crystallization are also very different. For bulk samples crystallizing from the melt where nucleation is naturally heterogeneous, waxes do not exhibit supercooling ($\Delta T < 0.05$ °C),[6] while PE supercools ~20 °C. Emulsified *n*-alkanes in the range $17 \le n \le 30$ exhibit homogeneous nucleation at undercoolings of ~14 °C[7−10] while PE does not exhibit homogeneous nucleation until undercoolings of ~60 °C are reached.[11,12] The difference in these values had been attributed to the large energy of the chain-fold surface at large *n*, compared to the much lower energy of the CH_3- surface at small *n*.[11] The crossover is then expected to relate to the onset of chain folding. Here we investigated the crossover in the characteristic undercooling exhibited for homogeneous nucleation (ΔT) and show the unexpected result that the increasing trend begins by $n = 25$ and is thus unlikely to be associated with chain folding.

We will argue that *if* shorter *n*-alkanes have critical nuclei consisting of full molecules, then by $n \approx 25$, there must be a crossover from a nucleus consisting of full molecules whose surface is terminated by CH_3- groups to a nucleus consisting of a bundle of ordered $-CH_2-$ sequences without the chains terminating at the nucleus' surface. However, we show that the behavior of the kinetic prefactor is more consistent with a change to a bundle (i.e., *n* rising above m_c, the thickness of the critical nucleus in $-CH_2-$ units) already having occurred by $n \sim 18$. We then show that the increases in ΔT and the interfacial energy, σ, beginning between $20 < n < 30$ occur when *n* rises above $m_c + 2C_\infty$ (where C_∞ is the characteristic ratio, related to the persistence length in $-CH_2-$ units). In contrast with previous arguments,[13−15] the uncrystallized chain ends (cilia) attached to a bundle or "fringed-micelle" nucleus will not create an entropic cost until they exceed a characteristic length. Here we invoke a similar argument to that used by Turnbull and Spaepen to explain the solid−liquid surface energy of short alkanes[16] and by Hoffman and collaborators regarding the lateral surface energy of polyethylene.[17−19] The extrapolation of ΔT and σ toward the values for PE suggests that the fringed-micelle picture of the critical nucleus, discarded long ago, may warrant revisiting.

Background

Measurements of homogeneous nucleation, using the droplet method developed by Vonnegut,[20] were first performed on alkanes and polyethylene by Turnbull and collaborators.[9,11] Small emulsion droplets of the sample are prepared in a dispersing medium by use of a surfactant. Thus, when a crystal nucleates in a single droplet, it rapidly grows and crystallizes only that one droplet but does not affect the other droplets.[21] The other feature of emulsions is the removal of macroscopic heterogeneities as nucleators in the system. For example, if a dust particle were to be a nucleator, then in

[†] Bar Ilan University.
[‡] ExxonMobil Research and Engineering Co.
* Corresponding author. e-mail: ebsirot@erenj.com.

10.1021/ma000312m CCC: $19.00
Published on Web 07/19/2000

a bulk sample (i.e., not an emulsion) it would cause crystallization of the whole sample. However, in an emulsion it would only crystallize one droplet, which would be insignificant. The emulsions thus also remove the effect of walls and of liquid−vapor interfaces both at the surface and at ubiquitous bubbles. This is important, especially for *n*-alkanes where the liquid−vapor interface exhibits surface crystallization and is believed to cause heterogeneous nucleation yielding a negligible supercooling in bulk samples.[6,22,23]

The undercooling required for homogeneous nucleation of high-MW polyethylene is ∼58 °C.[11,12,24] The undercoolings for *n*-alkanes of $15 < n < 30$ are ∼14 °C and do not vary significantly with chain length.[7−10] This is considered a somewhat "anomalous" regime since $\Delta T/T$ is ∼0.05, which is substantially less than that exhibited by most other materials. These low undercoolings could be partly attributed to the very low surface energy of the chain-end methyl interfaces against the liquid of *n*-alkanes, a property which also manifests itself in the surface crystallization effect exhibited by alkanes with $15 < n \leq 50$.[22,25−27] For shorter *n*, the undercooling increases with decreasing *n*, producing a crossover from chain-molecule behavior to that of a simple molecules such as methane. This low-*n* crossover has been explained by the negentropic model of Turnbull and Spaepen.[16] In that model, which employs a spherical nucleus, the surface energy at the solid−liquid interface is considered to arise from the entropic constraints on the molecules in the liquid phase near the crystalline surface. Since there is some correlation in the ordering of connected neighboring segments, the crossover to "large-*n*" (i.e., $n > 15$) behavior in this respect has a typical length. Hoffman et al. have related this to the characteristic ratio C_∞ or the Kuhn length in polymers.[17−19]

Our interest here, however, is the other crossover (at larger chain lengths) to the polymer behavior where the undercoolings and surface energies rise again. The difference in the observed homogeneous undercooling and derived surface energies is usually attributed to the higher energy of the chain-folded surface ($\sigma_e \sim 90$ dyn/cm),[11,15,17] as compared to the methyl-end surface of an *n*-alkane crystal where σ_e may be as low as 1−3 dyn/cm.[27] The low energy of that methyl surface,[28] at both a liquid and vapor interface, has been argued to be responsible for the surface crystallization effect seen in *n*-alkanes.[27]

For the comparisons here, we will use our recent homogeneous nucleation data on *n*-alkanes ($17 \leq n \leq 60$)[10] and the polyethylene data of Ross and Frolen (RF), which is a consistent set of nucleation kinetics data over a variation of molecular weight.[12] Over the ranges of overlap, our *n*-alkane data are consistent with the previous work of Turnbull and Cormia,[9] Uhlmann et al.,[7] and Oliver and Calvert.[8] Our results extend to almost twice the carbon number of the previous work but omit the chain lengths shorter than $n = 17$. We also report data on some low-MW PE fractions. For the polyethylene, the original work was due to Cormia, Price, and Turnbull,[11] and other studies have also been performed.[29,30]

Theoretical Background. Within the formalism of classical nucleation theory,[9,31] the homogeneous nucleation rate, in events per unit volume per unit time, is given by $I = K_v \exp[-W^*/RT]$. K_v is the kinetic prefactor which is related to the diffusion constant and represents the rate of "attempts" at forming a critical nucleus by sampling different configurations in the ensemble of possible configurations of the liquid. W^* is the nucleation barrier which represents the free energy of the "critical nucleus". When the free energy of a crystallite is written as a function of size, below the equilibrium melting temperature there is a negative term from the bulk free energy driving the crystal to grow ($\Delta S \Delta T$) and a positive term from the solid−liquid interfacial energy favoring shrinkage. There is a size at which the free energy is maximum and will decrease with subsequent growth. A nucleus of this size is called the "critical nucleus", its radius "the "critical radius", and its free energy the nucleation barrier W^*. The simplest model is that of a "spherical nucleus" where the solid−liquid interfacial energy is independent of the crystal face. In this case the nucleation rate is $I = K_v \exp\{(-16\pi\sigma^3/3\Delta S^2 \Delta T^2 RT)][(T + T_m)^2/(2T)^2]\}$ where σ is the interfacial energy, $\Delta T = T_m - T$ where T_m is the melting temperature and ΔS is the melting entropy. The term $((T + T_m)/2T)^2$, which is necessary at large undercoolings, is needed to account for the higher entropy of the liquid phase.[32] As we will discuss in more detail below, it is very important to realize that the phase into which nucleation occurs may not be the crystalline state finally observed. If nucleation occurs into a transient state, then one must use T_m and ΔS_m for the melting of the transient phase, not the stable phase.

While the spherical model allows us to extract an "effective σ" from kinetic data, the well-known structural and growth-rate anisotropy of both short *n*-alkanes and PE make the need for allowing independent "side" and "end" energies obvious. This is accomplished using the "cylindrical model".[7] We write the free energy in terms of the number of units in height *m*, and the radius *r*.

$$\Delta G = 2\pi r^2 \sigma_e + 2\pi r m d \sigma_s - \pi \Delta S \Delta T r^2 m d$$

where *d* is the units' (molecule or monomer) length, σ_e is the "end" surface energy/area of the solid−liquid interface at the surface of the layers, and σ_s is the "side" energy/area along the molecular sides. ΔS is the entropy of melting per unit volume, and $\Delta T = T_m - T$ is the undercooling below the equilibrium melting temperature of the phase which is nucleating.

To find the critical nucleus size, we look for the *lowest* maximum of ΔG as a function of *m* and *r* which must be crossed to get to large *m* and *r*. This is a saddle point at

$$m_c = 4\sigma_e/d\Delta S \Delta T \tag{1}$$

and $r_c = -2\sigma_s/\Delta S \Delta T$. This is shown in a plot of ΔG versus *r* and *m* in Figure 1a. The free energy at the saddle point which corresponds to the nucleation barrier is thus

$$\Delta G^* = \frac{8\pi \sigma_s^2 \sigma_e}{(\Delta S \Delta T)^2} \tag{2}$$

This expression corresponds to the spherical approximation replacing

$$\sigma_s^2 \sigma_e \leftrightarrow \frac{2}{3}\sigma^3 \tag{3}$$

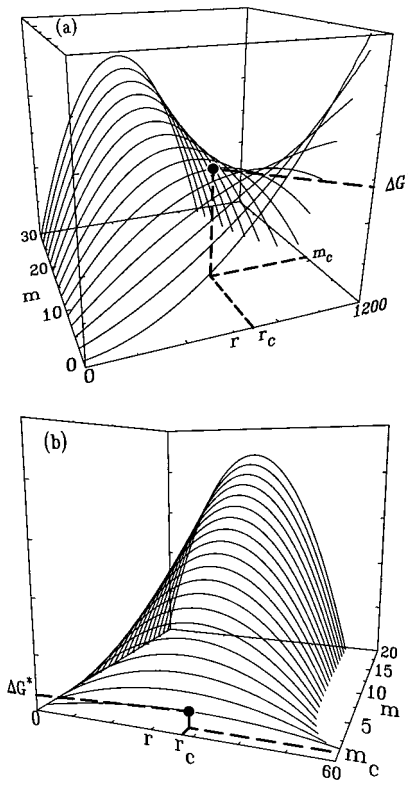

Figure 1. Example of a calculated ΔG for the cylindrical model with $\sigma_s d/\sigma_e = 150$ Å. (The z scale is not shown, but the $x-y$ plane is $\Delta G = 0$.) (a) The saddle point is illustrated choosing $d\Delta S\Delta T/\sigma_e = 0.4$. (b) The $m_c = 1$ case is illustrated choosing $d\Delta S\Delta T/\sigma_e = 10$. In both cases the effective minimum is shown by a solid point, the coordinates of which are marked by the subscript c. ΔG^* is the corresponding nucleation barrier.

However, if $m_c < 1$, then the saddle point cannot be reached while maintaining the CH_3- end surfaces. This is the case for $d\Delta S\Delta T > 4\sigma_e$. Here, one is limited to $m_c = 1$, and the lowest barrier is found to be

$$\Delta G_1^* = \frac{\pi d^2 \sigma_s^2}{(d\Delta S\Delta T - 2\sigma_e)} \tag{4}$$

with $r_c = d\sigma_s/(d\Delta S\Delta T - 2\sigma_e)$ as obtained by Uhlmann.[7] This situation is shown in Figure 1b.

Which Phase Is Nucleating? The difference between the nucleation temperature and the equilibrium melting temperature of the *stable crystal phase*, $\Delta T = T_m - T_s$, is one quantity which is a clear experimental observable. However, to calculate surface energies from nucleation measurements, one needs the thermodynamic parameters (ΔS_m and T_m) for the *phase into which nucleation is occurring*. For the *n*-alkanes and polyethylene, one must consider the fact that nucleation may occur into a transient metastable phase, in particular the rotator or hexagonal phases. For polyethylene, this point has been argued extensively by Keller et al.[33−42] An equilibrium hexagonal phase is known to occur in PE at high pressures above the triple point near $P = 3$ kbar.[43] However, the quantitative values for ΔS_{hl} and T_{hl} for such a metastable transition at $P = 1$ bar are not known. Furthermore, extrapolated behavior from either low n or high P where the rotator/hexagonal phase is stable give conflicting results and are therefore uncertain. Extrapolation to zero irradiation of the melting of the hexagonal phase of irradiated polyethylene also results in large uncertainty.[44] On the other hand, for the *n*-alkanes of $n \leq 60$, the metastable transition temperature can be reasonably well determined since extrapolation from regions of rotator phase stability is still rather small.[10]

For heterogeneous nucleation in bulk samples (i.e., macroscopic and unemulsified), it was recently shown that short *n*-even *n*-alkanes do nucleate via a transient metastable rotator phase before converting into their stable triclinic crystal.[23] In addition, C23 crystallizing from solution in C12 was shown to also nucleate via a transient metastable rotator phase before converting into the stable orthorhombic form.[45] Homogeneous nucleation of odd-length alkane droplets of $n \leq 19$ is known to occur into the rotator phase. This is obvious, since the crystals actually grow in the rotator phase, and the transition to the stable orthorhombic form occurs as a separate event which is clearly distinguishable in the experiment.[8−10,46] The fact that the homogeneous nucleation temperature T_s, the melting temperature of the rotator phase T_{rl}, and therefore their difference ΔT_r do not exhibit an odd−even effect, while T_{xl} and ΔT_x do, strongly suggests that homogeneous nucleation for the even-*n* in this chain-length range is also through a transient metastable rotator phase. Homogeneous nucleation into the rotator phase thus undoubtedly must occur for at least some range in $n > 21$, possibly, although not necessarily, all the way to PE. From homogeneous nucleation theory one can compute that nucleation will occur into the metastable rotator phase if $\sigma_{rl}^3/[\Delta S_{rl}(T - T_{rl})]^2 < \sigma_{xl}^3/[\Delta S_{xl}(T - T_{xl})]^2$ (where each σ^3 is really $^3/_2\sigma_s^2\sigma_e$ for a cylindrical nucleus).[23] Unfortunately, there is insufficient data available on the surface energies (both σ_s and σ_e) with distinction between the rotator−liquid (rl) and crystal−liquid (xl) interfaces.[27]

Results

Two types of measurements can be used to obtain nucleation kinetic data on such systems. Isothermal measurements using a probe which is integral in nature (i.e., microscopy, volumetrics, X-ray scattering) measure the fraction that *is crystalline* as a function of time, yielding a nucleation rate for each isothermal experiment. Calorimetry measures the derivative, or the number of droplets *crystallizing* (nucleating) per unit time: Thus, a shallow quench isothermal experiment would yield a negligibly small signal. Oliver and Calvert[8] developed a method for obtaining nucleation rate constants within the context of classical nucleation theory using constant cooling rate calorimetric data.

***n*-Alkane Data.** We carried out such constant cooling rate experiments using a specially designed calorimeter. The calorimeter consists of a copper sample cell suspended by thin Teflon strips inside an aluminum enclosure, the temperature of which is controlled and scanned at a constant rate. The *n*-alkane samples were obtained from Aldrich (labeled ≥99% pure) and were used as obtained. The emulsions were prepared using 0.25 g of alkane, 6 g of water, and 0.3 g of the nonionic surfactant Igepal CA-630 or CO-890. For the longest alkanes ethylene glycol was added to help kinetically stabilize the emulsion and was shown not to affect the observed undercooling. The samples were mixed with a magnetic stirbar on a hot plate to form an emulsion. The droplet size distribution was measured with light microscopy before and after nucleation measurements

Table 1. Data Summary for Homogeneous Nucleation of the *n*-Alkanes[a]

n	T_m	T_{rl}	T_{xl}	T_s	ΔT_m	ΔT_r	ΔT_x	σ_R	σ_{eR}	σ_X	σ_{eX}	ΔS_{rl}	ΔS_{xl}	m_{cR}	m_{cX}	σ_{sR}	$\Delta \log K_v$
17	21.6	21.6	19.2	8.2	13.4	13.4	11.0	6.1	1.09	6.4	1.3	0.572	0.728	5.1	5.4	7.6	1.7
18	28.2	27.0	28.2	13.8	14.4	13.2	14.4	5.7	0.89	8.3	2.7	0.550	0.804	4.4	7.9	6.9	1.5
19	31.8	31.8	29.6	18.5	13.3	13.3	11.1	5.8	0.94	6.4	1.3	0.531	0.700	4.7	5.5	7.1	1.8
20	36.3	36.0	36.3	22.6	13.7	13.4	13.7	5.7	0.89	8.0	2.4	0.523	0.795	4.5	7.6	7.0	2.1
21	40.1	40.1	38.1	26.5	13.6	13.6	11.6	5.8	0.94	6.6	1.4	0.517	0.699	4.8	5.8	7.2	2.5
22	43.8	43.8	43.5	30.2	13.6	13.6	13.3	5.9	0.99	8.0	2.4	0.511	0.788	5.1	7.9	7.4	2.9
23	47.2	47.2	45.3	33.4	13.8	13.8	11.9	5.8	0.94	6.8	1.5	0.506	0.715	4.8	6.0	7.2	3.0
24	50.4	50.4	49.5	36.3	14.1	14.1	13.2	5.9	0.99	7.9	2.4	0.501	0.782	5.0	7.7	7.4	3.3
25	53.3	53.3	51.4	39.0	14.3	14.3	12.4	6.0	1.04	7.2	1.8	0.497	0.724	5.2	6.8	7.5	3.7
26	56.0	56.0	54.9	41.6	14.4	14.4	13.3	6.0	1.04	7.9	2.4	0.493	0.761	5.2	7.9	7.5	3.9
27	58.6	58.6	56.9	43.6	15.0	15.0	13.3	6.1	1.09	7.6	2.1	0.490	0.719	5.3	7.4	7.6	4.1
28	60.9	60.9	59.8	45.4	15.5	15.5	14.4	6.3	1.20	8.3	2.7	0.487	0.756	5.6	8.4	7.9	4.6
32	68.8	68.8	68.1	52.1	16.7	16.7	16.0	6.6	1.37	8.6	3.0	0.485	0.718	6.0	8.8	8.1	5.3
33	70.9	70.9	70.1	53.6	17.3	17.3	16.5	6.7	1.43	8.8	3.2	0.485	0.718	6.0	9.1	8.2	5.3
36	75.4	75.4	74.9	56.3	19.1	19.1	18.6	7.2	1.76	9.5	4.1	0.485	0.718	6.7	10.4	8.6	5.9
37	76.8	76.8	76.6	57.2	19.6	19.6	19.4	7.2	1.76	9.6	4.3	0.485	0.718	6.5	10.3	8.4	5.7
40	80.9	80.8	80.9	59.0	21.9	21.8	21.9	8.0	2.47	10.8	6.0	0.485	0.718	8.3	12.8	9.4	6.9
41	82.3	82.1	82.3	59.6	22.7	22.5	22.7	8.2	2.66	11.1	6.5	0.485	0.718	8.6	13.3	9.5	7.1
42	83.6	83.3	83.6	60.2	23.4	23.1	23.4	8.0	2.47	10.9	6.3	0.485	0.718	7.8	12.5	9.0	6.3
44	85.5	84.9	85.5	61.3	24.2	23.6	24.2	8.5	2.94	11.6	7.5	0.485	0.718	9.1	14.5	9.6	7.3
46	88.0	87.1	88.0	62.4	25.6	24.7	25.6	8.8	3.25	12.1	8.5	0.485	0.718	9.5	15.4	9.7	7.5
48	89.9	88.7	89.9	62.9	27.0	25.8	27.0	8.9	3.35	12.3	8.9	0.485	0.718	9.4	15.3	9.5	7.2
50	91.9	90.4	91.9	64.1	27.8	26.3	27.8	9.2	3.68	12.8	9.9	0.485	0.718	10.1	16.6	9.8	7.7
54	95.3	93.2	95.3	65.5	29.8	27.7	29.8	9.4	4.03	13.4	11.5	0.485	0.718	10.5	18.0	9.7	7.7
60	99.7	96.7	99.7	67.8	31.9	28.9	31.9	9.8	4.54	14.1	13.3	0.485	0.718	11.3	19.3	9.6	8.0

[a] T in °C and σ in dyn/cm. T_m is the actual bulk melting temperature. T_{rl} and T_{xl} are the equilibrium or metastable melting temperatures of the rotator and crystal phases, respectively. T_s is the peak nucleation temperature on cooling at 0.2 °C/min. $\Delta T_m = T_m - T_s$, $\Delta T_r = T_{rl} - T_s$ and $\Delta T_x = T_{xl} - T_s$. σ_R and σ_X are computed with the spherical model assuming nucleation into the rotator and crystal phase, respectively. σ_{eR} and σ_{eX} are the end-surface energies calculated assuming $\sigma_s = 11.8$ dyn/cm for both the rotator and crystal phase. ΔS_{rl} and ΔS_{xl} are the melting enthalpies used in the calculations. m_{cR} and m_{cX} are the thicknesses of the critical nucleus in $-CH_2-$ units, assuming $\sigma_s = 11.8$ dyn/cm and bundle type nuclei. σ_{sR} is calculated assuming full molecule $m_c = 1$ nucleation into the rotator phase with $\sigma_e = 3$ dyn/cm. $\Delta \log K_v$ is the increase in the computed log K_v when imposing the $m_c = 1$ limitation.

and was found to follow a log-normal distribution with a mean diameter of 4−5 μm.

Cooling runs were performed at 0.2 °C/min. We extracted the temperature at which the peak crystallization rate was observed, T_s. The data were then fit using the procedure of Oliver and Calvert.[8] The kinetic prefactor K_v and surface energy were extracted with the knowledge of the melting temperature and entropy of the nucleating phase. Another procedure involving integration over the size distribution of the droplets, derived from the work of Herhold et al.,[47] was also used. This gave consistent results. Additional details of the sample preparation, experimental procedure, and data analysis procedures are presented elsewhere.[10]

As discussed above, to derive a surface energy or undercooling from such data, one must assume that one knows the properties of the phase that is nucleating. Since, for most of these chain lengths, it is conceivable that nucleation may be into either the rotator phase or the stable crystal phase, we computed the parameters assuming both possibilities. To do this, we needed thermodynamic data for both the melting of the rotator phase (T_{rl} and ΔS_{rl}) and melting of the crystal phase (T_{xl} and ΔS_{xl}). While only one of these is directly measurable for any given alkane, we used the relation $(T_{xl} - T_{xr})\Delta S_{xr} = (T_{rl} - T_{xl})\Delta S_{rl}$ to obtain the missing values. Here T_{xr} and ΔS_{xr} refer to the crystal−rotator transition, so $\Delta S_{xl} = \Delta S_{xr} + \Delta S_{rl}$. Supplementing the literature data[48−50] with our own data and interpolating and extrapolating where necessary, we obtained a consistent set of these parameters for $17 \leq n \leq 60$. These values for T_{rl}, T_{xl}, ΔS_{rl}, and ΔS_{xl} are shown in Table 1. The details of their determination have been previously presented.[10]

The following quantities are included in Table 1: The melting temperature T_m is the melting temperature of the equilibrium phase, and either corresponds to rotator melting T_{rl} or crystal melting T_{xl}. T_s is the nucleation temperature determined as the peak crystallization rate while cooling the emulsion at 0.2 °C/min. The undercoolings $\Delta T_m = T_m - T_s$, $\Delta T_r = T_{rl} - T_s$, and $\Delta T_x = T_{xl} - T_s$ are with respect to the equilibrium melting temperature, the rotator melting temperature, and the crystal melting temperature (be they stable or metastable), respectively. Using the spherical model, the surface energy is calculated both assuming nucleation into the rotator phase (σ_R) and into the crystal phase (σ_X).

We should not confuse σ_R and σ_X that we report here for the surface energies of the two respective phases; they are not. They are only the surface energies computed assuming that the nucleation we are measuring is into the rotator or the crystal phase. If nucleation is into the rotator phase, then σ_R would be the correct value for the surface energy of the rotator−liquid interface. However, σ_X would be meaningless, not the value of the actual crystal−liquid interface. The reverse is also true.

We therefore realize the large potential ambiguities in the calculated values of quantities such as σ, σ_e, and m_c. It is for this reason that these values and the thermodynamic values used to compute them are given in the tables, should the reader wish to compare these results to calculations with other assumptions.

Employing the same set of data but using the cylindrical model gives us one more unknown and thus requires us to know one more parameter. A reasonable choice is to assume that σ_s, the energy of the side surface, is temperature and chain length independent (for $n \geq 17$) and takes on the value of 11.8 erg/cm^2.[17] This is not to say that we believe that there is no n or T dependence. But assuming here any more variation

Table 2. Summary of Our Analysis of Ross and Frolen's Fractionated Polyethylene Homogeneous Nucleation Data[12] [a]

											σ−hexagonal; ΔS_{rl} =				
n	T_m	T_s	ΔT	σ	σ_e	log K_v	log I_0	$\sigma(T_s)$	$\sigma_e(T_s)$	T_{mH}	ΔS_{xl}	$0.75\Delta S_{xl}$	$0.25\Delta S_{xl}$	125 − T_s	m_{cX}
654	140.09	85.60	54.49	26.5	85.9	35.5	37.9	25.3	77.8	134.5	18.8	22.8	47.5	39.4	65.6
784	140.95	86.12	54.83	28.2	103.9	40.8	43.2	25.4	78.9	129.0	19.8	24.0	49.8	38.9	66.1
1264	143.15	86.09	57.06	30.3	129.1	46.1	48.5	26.0	84.0	125.5	20.5	24.8	51.6	38.9	67.7
1836	143.60	86.82	56.78	30.3	129.0	46.4	48.8	25.9	83.6	125.0	20.3	24.6	51.2	38.2	67.7
2598	144.17	87.49	56.68	29.7	120.7	44.1	46.5	25.9	83.6	127.0	19.7	23.9	49.6	37.5	67.8
6757	144.96	87.40	57.56	31.1	138.8	48.4	50.8	26.1	84.9	124.0	20.4	24.7	51.3	37.6	67.8
12750	145.21	87.40	57.81	31.3	142.3	49.1	51.5	26.3	87.2	123.5	20.4	24.8	51.5	37.6	69.4

[a] T in °C and σ in dyn/cm. n is derived from the weight-average MW. T_m is calculated from Broadhurst's[54] equation for $T_m(n)$, but assuming $T_m(\infty) = 145.5$ °C. T_s is the calculated peak nucleation temperature if the sample were cooled at 0.2 °C/min. $\Delta T = T_m - T_s$. σ is the surface energy assuming the spherical model. σ_e is the end surface energy assuming $\sigma_s = 11.8$ dyn/cm. K_v is the complete kinetic prefactor, and I_0 is one of its terms described in the text. $\sigma(T_s)$ and $\sigma_e(T_s)$ are the spherical model and cylindrical model end-surface energies at T_s, accounting for the temperature dependence imposed by assuming that log $I_0 = 34$. T_{mH} is the melting temperature which gives log $I_0 = 34$ in the absence of a temperature-dependent σ. σ-hexagonal is computed using the spherical model, assuming nucleation into a metastable hexagonal phase which melts at 125 °C and where $\Delta S_{rl} = \Delta S_{xl}$, $0.75\Delta S_{xl}$, or $0.25\Delta S_{xl}$. 125 − T_s represents $T_{mH} - T_s$. m_{cX} is the thickness of the critical nucleus in $-CH_2-$ units assuming orthorhombic nucleation with $\sigma_s = 11.8$ dyn/cm.

Table 3. Parameters from Low-MW PE Samples[a]

n_n	n_w	T_{mExp}	T_s	n_{AVG}	T_{mAVG}	ΔT
36.7	39.9	79.8	56.2	38.3 ± 1.6	78.2 ± 2.7	22.0
49.2	57.0	92.1	63.8	53.1 ± 3.9	94.1 ± 3.6	30.3
68.4	82.0	108.5	73.2	75.2 ± 6.8	106.8 ± 3.0	33.6
133.3	153.3	121.5	75.5	143.3 ± 9.9	123.1 ± 1.6	47.6

[a] n_n and n_w are the number- and weight-averaged carbon numbers. T_{mExp} is the measured peak melting temperature of unemulsified samples. T_s is the peak nucleation temperature on cooling the emulsions at 0.2 °C/min. n_{AVG} is the effective carbon number used in the plots. T_{mAVG} is an effective melting temperature discussed in the text. ΔT is the characteristic undercooling required to nucleate the emulsion.

would just add more unknown parameters to the discussion. (We note that the negentropic model[16] would predict σ constant in n for large n and proportional to absolute temperature since it is entropic in origin.)

Another uncertainty that arises with this choice in σ_s is whether it applies to the "side" surface of the orthorhombic crystal phase or of the rotator phase. If it is assumed to apply to the crystal phase, then we have no value for the rotator phase surface. There is, however, some ambiguity regarding which phase this surface energy represents: It is possible that it actually applies to the rotator phase since it is derived from growth measurements.[17] Even though the equilibrium phase may be the orthorhombic crystal, it is possible that the lateral growth fronts are in the rotator/hexagonal phase.[51,52] We, therefore, perform our calculations using $\sigma_s = 11.8$ erg/cm^2, acknowledging the ambiguities involved.

Low-MW Polyethylene Data. Here we include a preliminary account of low-MW polyethylene nucleation data measured in our laboratory. A more detailed discussion of these samples along with X-ray data will be reported elsewhere.[53] The four PE fractions were hydrogenated polybutadiene polyethylene standards obtained from Scientific Polymer Products Inc. of Ontario, NY. Their reported number- and weight-average MWs, converted to carbon number (n_n and n_w), are listed in Table 3.

The two lowest-n PE samples were emulsified according to the procedures described above[10] for the longer-n alkane samples. The two higher-n PE emulsions were prepared following the procedure of Cormia et al.[11] and RF.[12] The PE was repeatedly melted and recrystallized in nitrobenzene while stirring. The resultant PE microspheres were then separated in a centrifuge and redispersed in Igepal 630CA. In Table 3, we list the peak

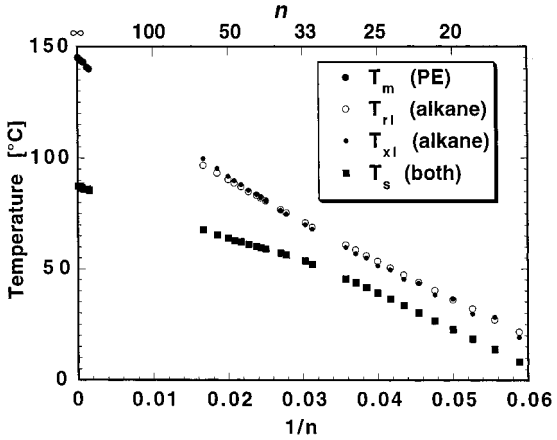

Figure 2. Equilibrium melting temperatures and the homogeneous nucleation crystallization temperature (T_s) of the PE and the n-alkanes versus 1/n. For the n-alkanes, both T_{rl} and T_{xl} are plotted, the higher of the two being the actual observed melting temperature (T_m).

melting temperatures of the unemulsified material (T_{mExp}) and the peak nucleation temperature on cooling the emulsified sample (T_s).

The distribution of carbon number is reflected in the large difference between n_w and n_n. This leads to the possibility of chain-length segregation in the crystal phase and the low-MW tail acting as a "solvent". We thus have to assign appropriate error bars to these data. This distinction is important when comparing to pure n-alkane data where n and T_m are well-defined. For determination of the equilibrium T_m, we used Broadhurst's equation[54] for $T_m(n)$ to determine T_{mAVG}, which is the average of $T_m(n_w)$ and $T_m(n_n)$. Our measured T_{mExp} is between these values. For n_{AVG} we considered n_w, n_n, and n as determined from our measured T_m. From these range of values we assigned error bars to n_{AVG} and T_m (thus ΔT). These are listed in Table 3 and plotted in Figure 3b.

Polyethylene Data from Ross and Frolen. The most detailed homogeneous nucleation droplet experiments on various MW fractions of polyethylene were performed by Ross and Frolen (RF).[12] While our measurements were performed at constant cooling rate and RF performed isothermal experiments, we can use their reported parameters to recast their results in terms of the same parameters measured in our study. In a constant cooling rate measurement, the simplest observable is the temperature of the peak in the crystal-

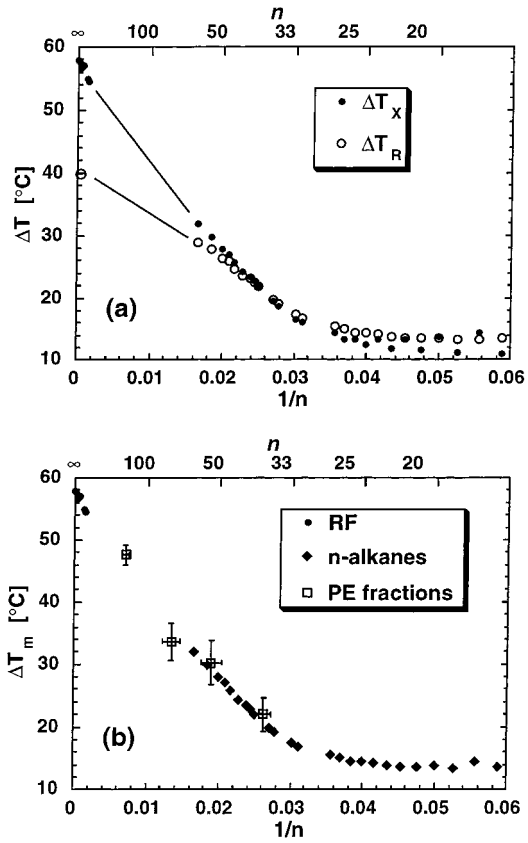

Figure 3. (a) Characteristic undercooling ($\Delta T = T_m - T_s$) for homogeneous nucleation of the polymers and the *n*-alkanes. For the *n*-alkanes, ΔT is shown with respect to both the rotator ($\Delta T_r = T_{rl} - T_s$) and the crystal ($\Delta T_x = T_{xl} - T_s$) phases. The higher of the two values is therefore with respect to the actual observed melting temperature. We also plot ΔT for PE assuming nucleation into a rotator (hexagonal) phase whose melting temperature is chosen as 125 °C, without chain-length dependence. (b) Undercooling with respect to the equilibrium melting temperature ΔT_m. Here, the low-MW PE samples are also included.

lization rate. This yields a characteristic nucleation temperature and thus a characteristic undercooling. Such a temperature is not explicitly defined in isothermal experiments which are performed over a range in temperatures, with higher temperatures yielding slower nucleation rates. However, the range in probed temperatures is narrow, since outside that range, crystallization is either too slow or fast to be measured. Thus, the range in temperatures over which isothermal measurements are reported will be close to the characteristic nucleation temperature associated with a constant cooling rate experiment. By using the reported prefactor and nucleation barrier obtained from the isothermal experiments, we can calculate the temperature at which the peak *would have* appeared, had their experiment been done by scanning temperature at a constant rate.

RF report the quantity I_0 which is related to K_v by $K_v = I_0 \exp[-U^*/R(T-T_\infty)]$, where $U^* = 1500$ cal/mol and $T_\infty = T_g - 30 = -50$ °C (the glass transition temperature, $T_g = -20$ °C).

$$I = K_v \exp\left[\frac{-30.2\sigma_s^2\sigma_e T_m^2}{\Delta h_f^2 \Delta T^2 RT}\frac{(T+T_m)^2}{(2T)^2}\right]$$

with $\Delta h_f = 290$ J/g. Using 1 μm for the average droplet radius and T_m, $\sigma_s^2\sigma_e$, and I_0 from RF's Table 2, the nucleation rate as a function of temperature could be computed and numerically integrated for a cooling rate of 0.2 °C/min. We then calculated the peak temperature (T_s in Table 2) in a hypothetical experiment with our conditions. To directly compare with our results, we convert RF's number-average MW to carbon-number *n*. We also tabulate the surface energy using the spherical model for nucleation $\sigma^3 = {}^3/_2\sigma_s^2\sigma_e$ and the full kinetic prefactor K_v.

RF noted that the prefactors are unphysically large when calculated under the assumption that the surface energies are constant in temperature. They then follow Hoffman et al.[55] in allowing a linear temperature dependence to the surface energies and fixing $\log(I_0)$ at a theoretical value of 34. RF then report $\sigma_s^2\sigma_e$ at T_m. Using this approximation and RF's temperature coefficients, we compute and tabulate $\sigma(T_s)$ at the *nucleation* temperature, which is somewhat lower than $\sigma(T_m)$. In their paper, RF assumed an $n = \infty$ PE melting temperature of 146.5 °C. The melting temperature is now believed to be 145.5 °C.[17] To account for the different T_m, we can replace ΔT by $\Delta T - \delta$ in the expression for the nucleation rate (here $\delta = 1$ °C). Expanding for $\delta \ll \Delta T$ allows us to replace σ^3 by $\sigma^3 = \sigma^3/(1 + 2\delta/\Delta T_0)$, where ΔT_0 is the nominal undercooling.

Another possible source of the unphysically large prefactor could be an incorrectly chosen melting temperature. If the critical nucleus is that of the metastable hexagonal phase, which is stable at high pressure as postulated by Keller et al.,[33-42] then the appropriate value to use for the melting temperature would be T_{mH}, which is $< T_{mO}$ (the equilibrium melting temperature of orthorhombic PE). Unfortunately, the position of the metastable phase boundary between the hexagonal phase and the melt is not precisely known at $P = 1$ bar. Keller suggested[36] $T_{mH} \geq 122-130$ °C. From the parameters given by RF, we calculated the observed nucleation rate as a function of temperature over the range they measured and recalculated I_0 vs ΔT for varying T_m: Here we assumed a temperature-independent σ and chose T_m such that the prefactor $\log(I_0) = 34$. These values, denoted T_{mH}, are shown in Table 2. While they are not constant, they are near Keller's suggested range. Choosing then a midrange value of $T_{mH} = 125$ °C, we calculate σ with this assumption. However, we must also make a choice of ΔS for this transition, since if we assume that nucleation is from the liquid to the hexagonal phase, we must use ΔS_{rl} and not ΔS_{xl}. Again, this value is unknown, and extrapolations are ambiguous. For low *P* and low *n* $\Delta S_{rl}/\Delta S_{rx} \sim 3/1$, while for high *P* and large *n* (high-pressure PE) $\Delta S_{rl}/\Delta S_{rx} \sim 1/3$.[48,56,57] Since it is not clear how to choose $\Delta S_{rl}/\Delta S_{rx}$ in the metastable low-*P*, high-*n* regime, we include in the table the calculated values of σ assuming $\Delta S_{rl} = \Delta S_{xl}$, $0.75\Delta S_{xl}$, and $0.25\Delta S_{xl}$.

It is clear that raising the issue of which phase is nucleating makes a model-dependent quantitative analysis of the data extremely ambiguous, because of the number of unknown thermodynamic parameters. The point is that further investigation is needed, especially regarding the nature of the possible metastable phase, to unambiguously obtain true interfacial energies.

Comparing Data. To show all the data on a single plot, we follow Dollhopf et al.[49] and use $1/n$ as the abscissa. This choice is not merely a convenience but has physical meaning in that $1/n$ is proportional to the chain-end density which distinguishes finite chains from

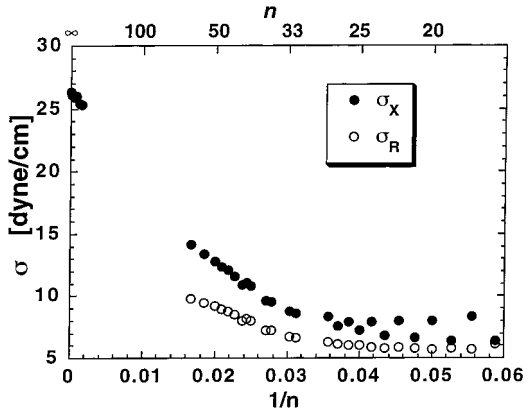

Figure 4. Spherical model effective surface energy $\sigma = (3\sigma_s^2\sigma_e/2)^{1/3}$ at T_s assuming nucleation into the crystal phase and also the rotator phase for the *n*-alkanes.

infinite polyethylene. In Figure 2, we plot as a function of $1/n$ our measured alkane nucleation temperatures T_s along with the PE values from RF. Also shown are the equilibrium melting temperatures T_m. For the alkanes, both the melting temperatures of the rotator and the crystal phases are shown, with the higher of the two being the equilibrium melting temperature. For PE, only the melting of the stable orthorhombic crystal is shown. The melting temperature of the metastable hexagonal phase may be ~125 °C[36] but is not exactly known. In Figure 3a we plot $\Delta T = T_m - T_s$ for both the polymers and the *n*-alkanes. Here, too, the ΔT for the *n*-alkanes is shown both with respect to the melting of the orthorhombic crystal ($\Delta T_x = T_{xl} - T_s$) and the rotator phase ($\Delta T_r = T_{rl} - T_s$). For PE, ΔT is shown with respect to the orthorhombic crystal melting as well as to a "hypothetical" melting temperature of the hexagonal phase at 125 °C (where *n* dependence was not included). It is clear that by $n = 25$, whether considering the orthorhombic or the hexagonal (rotator) phase, ΔT begins curving up from the constant value for $15 < n < 25$ in a way which appears to extrapolate toward the value for PE.

In Figure 3b, we plot ΔT with respect to the equilibrium bulk melting temperature (ΔT_m), whether it be the crystal or the rotator phase. Here we also include our data points from the four low-MW PE fractions, with their relatively large error bars. The points, nevertheless, show a trend consistent with the other data. We do not subject these four points to the further analysis of derived quantities such as surface energies, due to the larger uncertainties. For such studies, monodispersed high-MW *n*-alkanes would be required.[3]

In Figure 4 we plot the effective surface energy σ extracted from the spherical model. Again values are shown for *n*-alkanes with both assumptions of nucleation into the crystal phase (σ_X) and into the rotator phase (σ_R). The rotator phase values are calculated using the extrapolated ΔS_{rl} and T_{rl} which are given in Table 1. For PE, only σ for nucleation into the orthorhombic phase is shown here, since too many guesses of unknown parameters would be needed to obtain values assuming nucleation into the metastable hexagonal phase. For PE, where RF assumed a temperature-dependent σ, we plot its value at the nucleation temperature T_s. From this plot, too, it is apparent that there is an upturn in σ, beginning at $n \sim 25$, which tends to be extrapolating toward the value for PE by $n \sim 32$.

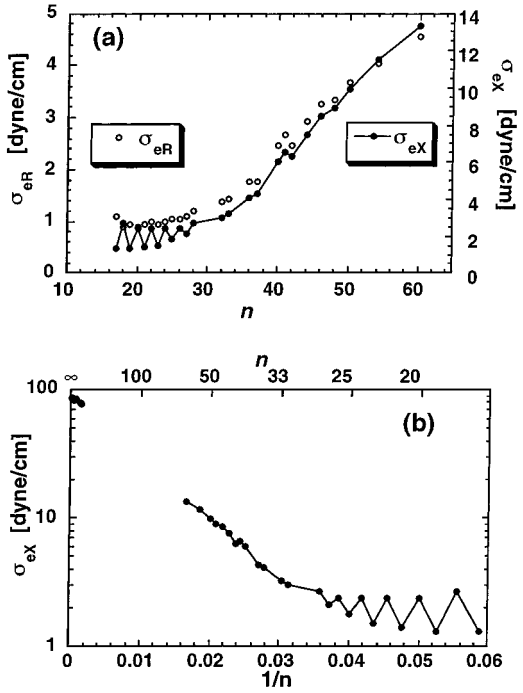

Figure 5. (a) End energy σ_e for the *n*-alkanes plotted versus *n*. Here we assume nucleation into either the rotator σ_{eR} or the crystal σ_{eX} phase, where $\sigma_s = 11.8$ dyn/cm assumed for both. (b) "End energy" σ_e at the nucleation temperature, calculated assuming nucleation into the crystal phase, assuming $\sigma_s = 11.8$ dyn/cm and allowing for the temperature dependence of σ_e in PE.

We can go a step further and use the cylindrical model to compute σ_e. To do this, we need to know σ_s. While we know that there will be undoubtedly *n* and *T* dependence for σ_s (with possibly very different values for the crystal and rotator phases), we compute σ_e using the single value of $\sigma_s = 11.8$ dyn/cm.[17] We include in Table 1 computations of σ_e using eq 3, assuming nucleation into the rotator phase with $\sigma_s = 11.8$ dyn/cm (σ_{eR}) and into the crystal phase with $\sigma_s = 11.8$ dyn/cm (σ_{eX}). In Figure 5a we plot σ_{eR} and σ_{eX} for $17 \leq n \leq 60$. Here, the increase above $n \sim 25$ is evident for *either* assumption. For PE, we also compute $\sigma_e(T_s)$ using eq 3, assuming nucleation into the crystal phase with $\sigma_s = 11.8$ dyn/cm (Table 2). In Figure 5b, we plot σ_{eX} vs $1/n$ for the alkanes and PE and observe the extrapolating trend again. However, here it appears more logarithmic than linear. Because of the significant uncertainties in the possible variation of σ_s and its affecting σ_e as $1/\sigma_s^2$, we will not try to ascribe any particular significance to this aspect of the curve. Note, however, that the upturn in the curve occurs near $n \sim 25$ regardless of whether a linear or logarithmic behavior is observed.

We can also compute the thickness of the critical nucleus within the same model (eq 1) and with the same high level of dependence on approximated parameters. In Table 1, we show m_c assuming crystal phase nucleation (m_{cX}) and rotator phase nucleation (m_{cR}) for the alkanes and m_{cX} for PE. These are plotted in Figure 6a,b. This again shows similar crossover behavior.

Looking at the values of m_c for the alkanes, we see that $m_c < n$ when the unit of *m* is the $-CH_2-$ monomer and when eq 2 is employed. This means that if we want to consider the nucleation mode where the full molecule is the unit and $m_c = 1$, we must use eq 4. We can do this without actually refitting the data.

The fitted parameter is essentially the slope of ΔG^* with respect to ΔT^{-2}. We define $\Omega = \partial \Delta G^*/d(\Delta T^{-2}) = 16\pi\sigma^3/3(\Delta S)^2$ and $\Omega_1 = \partial \Delta G_1^*/d(\Delta T^{-2}) = [\pi d^3 \sigma_s^2 \Delta S/(d\Delta S\Delta T - 2\sigma_e)^2](\Delta T^3/2)$.

Equating $\Omega = \Omega_1$, we obtain

$$\sigma_e = \frac{d\Delta S\Delta T}{2}\left(1 \pm \frac{\sigma_s}{4\sigma}\sqrt{\frac{3}{2}\frac{d\Delta S\Delta T}{\sigma}}\right) \qquad (5)$$

or

$$\sigma_s^2 = \frac{32}{3}\frac{\sigma^3(d\Delta S\Delta T - 2\sigma_e)^2}{(d\Delta S\Delta T)^3}$$

where σ is the original fitted value from the spherical model. The $\pm$ sign in eq 5 gives two solutions, and it is the negative sign which would represent the reasonable case where $\sigma_e < \sigma_s$. However, assuming $\sigma_s = 11.8$ dyn/cm and rotator phase nucleation, we obtain $\sigma_e < 0$, which is not physical. On the other hand, if we choose $\sigma_s \sim \leq 10$ dyn/cm, then reasonably small finite values of σ_e are obtained.

Similarly, the prefactor with the $m_c = 1$ assumption (K_{v1}) may be obtained from the existing fitted K_v using

$$\log K_{v1} = \log K_v + 0.4343(\Delta G_1^* - \Delta G^*)/kT \qquad (6)$$

In Table 1 we also include an example calculation of σ_s and $\log K_{v1} - \log K_v$ assuming $m_c = 1$ and guessing a constant $\sigma_e = 3$ dyn/cm.[27] Since the values of $\log K_v$ for $17 \leq n \leq 30$ are basically constant,[10] we see that eq 6 makes them increase slightly. Varying the value chosen for σ_e does not qualitatively alter this result. We will return to this point in the discussion.

Discussion

Our main point is that, despite an ambiguity of the phase into which nucleation is occurring, ΔT and σ begin a clear increasing trend for $n \geq 25$. When ΔT is plotted versus $1/n$, it appears to extrapolate linearly to the $n = \infty$ PE behavior. This strongly suggests that the mechanism involving the crossover from short *n*-alkane ("wax") behavior to high-*n* ("polymer") behavior is taking effect at chain lengths as low as $n = 25$. This seems to rule out chain folding as the main mechanism, as chain folding does not occur until much higher chain lengths.[3,5] There is a flat region $15 \leq n \leq 30$ where σ_e (and σ_s) are very low and roughly constant. For $5 \leq n \leq 15$ there is the sharply falling and leveling off which is explained by the negentropic model.[16] The low constant values of ΔT, σ, and σ_e, seem to suggest a very low energy end surface which is consistent with a CH_3- termination surface.[28] However, to accomplish this, the nucleus must consist of complete molecules. If nucleation is to involve entire extended-chain molecules, the combinatorial probability and thus the kinetic prefactor which involves rotational and translational diffusion would be highly reduced as the molecules become longer. On the other hand, the prefactor for nucleation of limited length bundles of sequences of $-CH_2-$ units would not decrease so strongly with increasing chain length.

Thus, if we consider two possible modes of homogeneous nucleation with different surface energies and kinetic prefactors, a crossover between the two modes is possible. Of course, since the nucleation rate depends exponentially on surface energy, the kinetic prefactor would have to vary by many orders of magnitude. Considering both the decreasing combinatorial probability of obtaining laterally packed molecules with ends in longitudinal registry, along with the diffusion constants (including those associated with rotating the entire molecules) which will affect how often different states can be sampled, such a prefactor decrease can be expected. A quantitative calculation of this is clearly warranted.

One possible mechanism for the crossover observed in the alkanes is a shift from critical nuclei consisting of full molecules with the very low energy CH_3- surfaces at the "end surface" to "bundle" nuclei, where the nucleus consists of only parts of the molecule. The crossover region, where *n* is still not too large, is still likely to contain nuclei whose interface contains some nonnegligible fraction of CH_3- groups.

Crystallization mediated by nucleation of unlayered bundles is also supported by crystallization studies of waxes by Dorset, in various long-chain naturally occurring waxes,[58,59] mixtures of long-chain *n*-alkanes (C50 and C60),[60] and a low-MW fractionated polyethylene (~average C43).[61] Dorset has shown that initial crystallization can be into a "crystalline nematic" state, where the chains crystallize without regard to the positions of their ends. When samples are crystallized by vapor deposition, and thus at a very low-temperature with respect to the melting point, there is insufficient mobility to reorganize. Upon annealing, the systems develop lamellar order, but where lamellae-spanning chains cause the lamellae repeat to be locked into an integral multiple of 1.27 Å, the projected carbon−carbon distance. Upon further annealing, the systems evolve to a state where the chain ends form the lowest energy surfaces separating the lamellae, and the repeat spacing is no longer locked into an integral multiple of 1.27 Å. This progression is shown schematically in Figure 7. This provides additional evidence that nucleation of the longer *n*-alkane waxes can occur without regard to the position of the chain ends in forming a low-energy surface.

Since the crossover in *n*-alkane behavior seems to extrapolate all the way to PE as ΔT implies, it suggests that the critical nucleus can be described as a "bundle" of aligned and properly packed, all-trans $-CH_2-$ chain segments. The critical bundle's length is not particularly defined by chain ends, or folds, but rather by where proper packing has ended. This picture of the critical nucleus is not new but rather had been proposed and discussed extensively decades ago, referred to as the "fringed micelle" or "bundle" nucleus.[15,62,63] This model for the critical nucleus was abandoned in favor of a folded-chain picture of the critical nucleus: This was due to arguments that calculations[13,14,64,65] of the effective surface energy of such a bundle nucleus ($\sigma_e \sim 250$ dyn/cm) was far in excess of the energy of a chain-folded surface ($\sigma_e \sim 90$ dyn/cm), the known state into which crystallization usually proceeds. However, one can certainly call into question such a high computed surface energy if one considers either of the two following possibilites: (1) the transition region or "interphase" might be similar to the hexagonal phase, which would be a local minimum in the free energy, or (2) the nucleus might be of the hexagonal phase itself, having a larger volume per $-CH_2-$ and a higher conformational entropy (see Figure 8).

We understand the essence of Zachmann's calculation[13,14] as follows: The "end" surface of such a critical

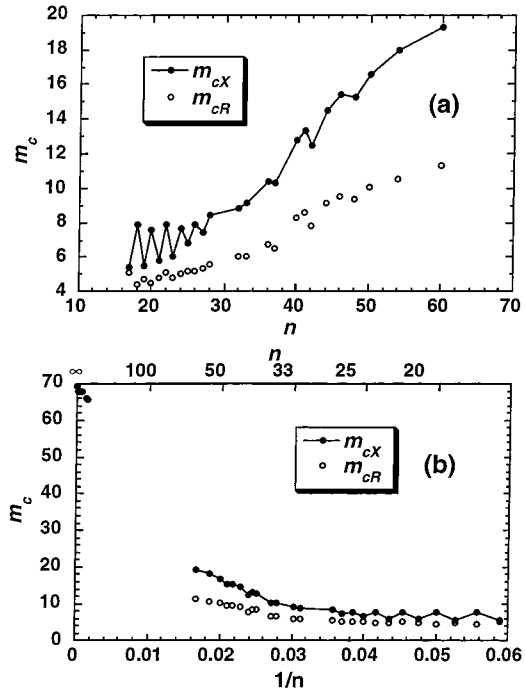

Figure 6. (a, b) Length of the critical nucleus (m_c in $-CH_2-$ units) at the nucleation temperature, assuming $\sigma_s = 11.8$ dyn/cm. It is calculated assuming both nucleation into the rotator and crystal phase. However, the same value of σ_s is used for both, since σ_s for the rotator phase is not known. m_c is shown for (a) the *n*-alkanes versus *n* and (b) together with PE versus $1/n$.

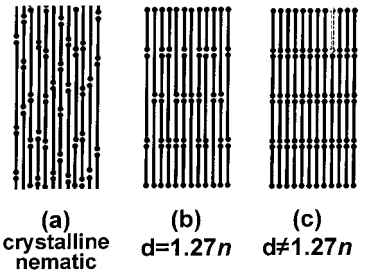

Figure 7. Schematic of the progression of lamellar order, based on work of Dorset:[58-61] (a) crystalline nematic, where there is no long-range lamellar order; (b) lamellae-spanning chains which make $d = 1.27n$ Å commensurate with the $-CH_2-$ repeat; (c) lamellae are fully segregated, and $d \neq 1.27n$ Å is incommensurate.

nucleus is not a real interface where the "liquid" segments could be separated from the ordered ones. He calculated the excess interfacial energy which was caused by the *entropic* constraints on the "liquid" segments by being connected to the "crystalline" ones and emanating nearly parallel from the virtual surface.[66] The liquid-to-crystal transition can be considered as a tradeoff of enthalpy and entropy: At the melting transition, the gain in conformational entropy is exactly canceled by the loss in the enthalpy of properly packed molecules which had optimized their van der Waals interactions. The change in both quantities is quite large, and thus a change in one without the canceling change in the other would give an enormous unphysical change in the free energy. Zachmann and others assumed that on one side of the interface the molecules have the enthalpy and entropy of the crystal phase, and beyond the "interface", the molecules have the fully highly unfavorable enthalpy of the liquid, but whose high liquid entropy is significantly constrained by the

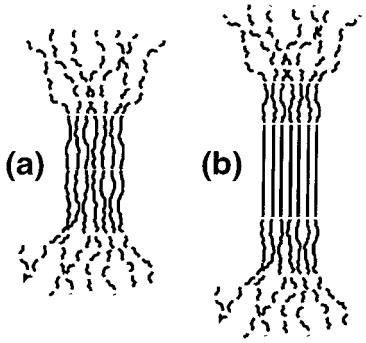

Figure 8. Schematic showing interphase morphologies which include hexagonal/rotator regions which may be expected to have a lower interfacial energy than sharp interfaces between crystal and amorphous. (a) The nucleus itself may be rotator/hexagonal. This is known to occur for low *n*. (b) A crystal nucleus with a rotator/hexagonal "interphase". The rotator phase may be a local minimum in the free energy.

connection of the molecules to the interface. It was only the reduction of the entropy which was calculated. The favorable contributions to the *enthalpy* resulting from the same constraints were not computed. Thus, the high value of $\sigma_e \sim 250$ dyn/cm is really a highly overestimated upper limit on σ_e.

The significant amount of unaccounted-for enthalpy is evidenced by the stability at higher pressure of the high-entropy hexagonal phase and presumably its metastability at lower pressures and temperatures. This phase has molecules with only part of the liquid's conformational entropy and, on average, directed parallel.[71] The fact that this phase can be stable shows that the enthalpic gain in such constrained but conformationally disordered structures can be *more than enough* to cancel the entropy deficit (relative to the liquid). Thus, the existence of the hexagonal phase in the general phase diagram shows that even though the favorable enthalpy may not make such a conformationally disordered but constrained structure a state of thermodynamic equilibrium at any given *T* or *P*, it may indeed bring its free energy very close to those of the liquid or crystal. It is, therefore, apparent that a valid calculation of the effective surface energy of the "end surface" of a bundle nucleus must take into account enthalpy, not just entropy. It must employ a model that can successfully predict the stability of the observed high-entropy, hexagonal phase.

We have argued that, for large *n*, nucleation may proceed as bundles, not complete molecules. We must ask, then, whether this crossover is indeed occurring in the vicinity of $20 \leq n \leq 30$, leading to the beginning of the observed rise in ΔT and σ. According to the arguments above, we would expect a strong decrease in K_v with increasing *n*, only leveling off after the nucleation mode crossed over from complete molecules to bundles of partial molecules. However, the K_v values that we have measured and reported over this range[10] appear to be roughly constant. Applying the "correction" (eq 6) to properly account for the $m_c = 1$ assumption self-consistently makes K_v *increase*, not decrease. Thus, the expected signature is absent here. (We do reiterate[10] that the K_v is the least experimentally reliable parameter, so the lack of an observed effect here might be an artifact.) On the other hand, Oliver and Calvert[8] measured prefactors that *do* show a strong decrease between $n = 10$ and $n = 18$, which is consistent with such a crossover. If this indeed occurs in that range, it

would complicate the quantitative interpretation of σ in terms of the negentropic model where only the spherical model was employed.[16] If the crossover from molecules to bundles has already occurred for smaller n, we then need another explanation for the rise in σ, which begins around $n \approx 25$.

As discussed above in relation to the work of Zachmann,[13,14] it is known that the constraints on the "liquid" chains connected to the critical nucleus will yield an entropic cost and, therefore, an increased σ. However, employing an argument analogous to those of Turnbull and Spaepen[16] and Hoffman,[17−19] we note that the "liquid" chains are still straight for a characteristic length. Thus, the increase in σ should begin when the molecules protrude from the nucleus beyond this length. If n_s is this characteristic length (in $-CH_2-$ units) which, as Hoffman et al. suggests, is closely related to the characteristic ratio C_∞ or C_n,[17−19] then we expect an increase in σ to begin when $n > m_c + 2n_s$.

In Table 1, for $n = 28$, we computed $m_c = 5.6$ and $\sigma_e = 1.2$ dyn/cm, assuming $\sigma_s = 11.8$ dyn/cm. Those values for σ_e and m_c may be somewhat low, as $\sigma_s = 11.8$ dyn/cm is the value for the crystal phase not the rotator. Lower values for σ_s are expected for the rotator phase, although they are not known. For instance, using $\sigma_s = 9$ (8) dyn/cm, we calculate $\sigma_e = 2.1$ (2.6) dyn/cm and $m_c = 9.7$ (12.3).

With $C_\infty = 6.7$,[72] we see that $m_c + 2C_\infty$ falls reasonably near $n \approx 25$, where σ and ΔT begin their increase. This bears some resemblance to the negentropic model[16] where the decrease in σ_s was argued to level off by $n \approx 2n_s + 2 \approx 14$, which implies that $n_s \approx 6$. In our case, σ_e increases beyond $n \approx m_c + 2n_s$.

Conclusions

We have shown that the crossover as a function of chain length from the lower constant undercooling for homogeneous nucleation to an increasing one takes place near $n \approx 25$. This increase at surprisingly low values of n, measured between $17 \leq n \leq 60$, appears to extrapolate to the high-n polyethylene behavior. This suggests that the mechanism responsible for this increase is not associated with chain folding, which does not set in until much larger n. This behavior suggests that low-energy CH_3- surface terminated nuclei may cross over to nuclei consisting of bundles of ordered $-CH_2-$ sequences organized without regard to the position of the molecular ends. In the long-chain limit, this is the "fringed micelle" picture. The observed crossover and the fact that short-n molecules nucleate into the rotator phase leads us to give serious consideration to the possibility of a metastable hexagonal phase playing a role in nucleating polytheylene. With these considerations, we find that the logic which previously led to the abandonment of the fringed-micelle nucleus neglected a potentially significant compensating enthalpy which may balance the high entropic cost.

We have proposed two possible reasons for the increase in undercooling occurring near $n \approx 25$: (1) a crossover in nucleation of entire molecules to nucleation of fractional molecule bundles occurring here; (2) the crossover to partial molecules occurs at a much lower n, and the increase in σ at $n \approx 25$ is due to the entropy cost of the dangling chains or cilia when $n > m_c + 2n_s$. The lack of a strongly decreasing kinetic prefactor between $17 < n < 30$ and evidence for such a strong decrease for lower n[8] leads us to favor the latter mechanism.

While we do not yet have a complete picture of alkane and polyethylene nucleation, it is clear that the "bundle" or "fringed-micelle" mode of primary nucleation needs serious reconsideration. Specifically, the full free energy cost associated with such an interface needs to be computed, for both orthorhombic and hexagonally ordered regions. It is essential to include the enthalpic van der Waals interactions. The test of the validity of any model used in such a calculation must be its ability to successfully predict the known properties of the hexagonal phase observed at high pressures. Such a model will not only help elucidate some of the remaining questions about the equilibrium hexagonal phase[71] but also allow calculation of the metastable phase boundaries. Such work will help facilitate a resolution of the mechanism for nucleation in polyethylene and the role, if any, of the metastable hexagonal phase.

Acknowledgment. We acknowledge enlightening discussions with Prof. J. D. Hoffman, D. Lohse, S. Srinivas, B. Hsiao, R. Kolb, A. B. Herhold, H. E. King, Jr., Y. Rabin, and S. T. Milner. We thank Exxon Research and Engineering Company for financial support of the work at Bar Ilan University.

References and Notes

(1) Keller, A. *Philos. Mag.* **1957**, *2*, 1171.
(2) Wunderlich, B.; Arakawa, T. *J. Polym. Sci., Part A* **1964**, *2*, 3697.
(3) Ungar, G.; Stejny, J.; Keller, A.; Bidd, I.; Whiting, M. C. *Science* **1985**, *229*, 386.
(4) Urabe, Y.; Tanaka, S.; Tsuru, S.; Fujinaga, M.; Yamamoto, H.; Takamizawa, K. *Polym. J.* **1997**, *29*, 534.
(5) Stack, G. M.; Mandelkern, L. *Macromolecules* **1988**, *21*, 510.
(6) Sirota, E. B. *Langmuir* **1998**, *14*, 3133.
(7) Uhlmann, D. R.; Kritchevsky, G.; Straff, R.; Scherer, G. *J. Chem. Phys.* **1975**, *62*, 4896.
(8) Oliver, M. J.; Calvert, P. D. *J. Cryst. Growth* **1975**, *30*, 343.
(9) Turnbull, D.; Cormia, R. L. *J. Chem. Phys.* **1961**, *34*, 820.
(10) Kraack, H.; Sirota, E. B.; Deutsch, M. *J. Chem. Phys.* **2000**, *112*, 6873.
(11) Cormia, R. L.; Price, F. P.; Turnbull, D. *J. Chem. Phys.* **1962**, *37*, 1333.
(12) Ross, G. S.; Frolen, L. J. *J. Res. Natl. Bur. Stand.* **1975**, *79A*, 701.
(13) Zachmann, H. G. *Kolloid Z. Z. Polym.* **1969**, *231*, 504.
(14) Zachmann, H. G. *Kolloid Z. Z. Polym.* **1967**, *216−217*, 180.
(15) Wunderlich, B. *Macromolecular Physics;* Academic Press: New York, 1976; Vol. 2.
(16) Turnbull, D.; Spaepen, F. *J. Polym. Sci.* **1978**, *63*, 237.
(17) Hoffman, J. D.; Miller, R. L. *Polymer* **1997**, *38*, 3151.
(18) Hoffman, J. D.; Miller, R. L.; Marand, H.; Roitman, D. B. *Macromolecules* **1992**, *25*, 2221.
(19) Hoffman, J. D. *Polymer Commun.* **1992**, *33*, 2643.
(20) Vonnegut, B. *J. Colloid Sci.* **1948**, *3*, 563.
(21) Herhold et al.[47] have shown that impurity migration out of droplets that crystallize and into uncrystallized droplets can lead to an effect where crystallization of some droplets impedes the crystallization of others.
(22) Ocko, B. M.; Wu, X. Z.; Sirota, E. B.; Sinha, S. K.; Gang, O.; Deutsch, M. *Phys. Rev. E* **1997**, *55*, 3164.
(23) Sirota, E. B.; Herhold, A. B. *Science* **1999**, *283*, 529.
(24) Gornick, F.; Ross, G. S.; Frolen, L. J. *J. Polym. Sci., Part C* **1967**, *18*, 79.
(25) Wu, X. Z.; Sirota, E. B.; Sinha, S. K.; Ocko, B. M.; Deutsch, M. *Phys. Rev. Lett.* **1993**, *70*, 958.
(26) Wu, X. Z.; Ocko, B. M.; Sirota, E. B.; Sinha, S. K.; Deutsch, M.; Cao, B. H.; Kim, M. W. *Science* **1993**, *261*, 1018.
(27) Sirota, E. B.; Wu, X. Z.; Ocko, B. M.; Deutsch, M. *Phys. Rev. Lett.* **1997**, *79*, 531.
(28) Zisman, W. A. Relation of the Equilibrium Contact Angle to Liquid and Solid Constitution. In *Contact Angle, Wettability and Adhesion*; Fowkes, F. M., Ed.; American Chemical Society: Washington, DC, 1964.
(29) Barham, P. J.; Jarvis, D. A.; Keller, A. *J. Polym. Sci.* **1982**, *20*, 1733.

(30) Koutsky, J. A.; Walton, A. G.; Baer, E. *J. Appl. Phys.* **1967**, *38*, 1832.
(31) Turnbull, D.; Fisher, J. C. *J. Chem. Phys.* **1949**, *17*, 71.
(32) Hoffman, J. D.; Weeks, J. J. *J. Chem. Phys.* **1962**, *37*, 1723.
(33) Hikosaka, M.; Rastogi, S.; Keller, A.; Kawabata, H. *J. Macromol. Sci.* **1992**, *B31*, 87.
(34) Hikosaka, M.; Amano, K.; Rastogi, S.; Keller, A. *Macromolecules* **1997**, *30*, 2067.
(35) Keller, A.; Goldbeck-Wood, G.; Hikosaka, M. *Faraday Discuss.* **1993**, *95*, 109.
(36) Keller, A. A Unifying Scheme for Polymer Crystallization. In *NATO ASI Series Vol. 405*; Dosiere, M., Ed.; Kluwer: Dordrecht, 1993.
(37) Keller, A.; Hilosaka, M.; Rastogi, S.; Toda, A.; Barham, P. J.; Goldbeck-Wood, G. *J. Mater. Sci.* **1994**, *29*, 2579.
(38) Keller, A.; Hikosaka, M.; Rastogi, S.; Toda, A.; Barham, P. J.; Goldbeck-Wood, G. *Philos. Trans. R. Soc. London A* **1994**, *348*, 3.
(39) Keller, A.; Rastogi, S.; Hikosaka, M. H. *Macromol. Symp.* **1997**, *124*, 67.
(40) Keller, A.; Hikosaka, M.; Rastogi, S. *Phys. Scr.* **1996**, *T66*, 243.
(41) Keller, A.; Cheng, S. Z. D. *Polymer* **1998**, *39*, 4461.
(42) Rastogi, S.; Hikosaka, M.; Kawabata, H.; Keller, A. *Macromolecules* **1991**, *24*, 6384.
(43) Bassett, D. C.; Turner, B. *Philos. Mag.* **1974**, *29*, 925.
(44) Ungar, G.; Keller, A. *Polymer* **1980**, *21*, 1273.
(45) Sirota, E. B. *J. Chem. Phys.* **2000**, *112*, 492.
(46) Herhold, A. B.; King, H. E.; Sirota, E. B., to be published.
(47) Herhold, A.; Ertas, D.; Levine, A. J.; King, H. E. *Phys. Rev. E* **1999**, *59*, 6946.
(48) Broadhurst, M. G. *J. Res. Natl. Bur. Stand.* **1962**, *66A*, 241.
(49) Dollhopf, W.; Grossmann, H. P.; Leute, U. *Colloid Polym. Sci.* **1981**, *259*, 267.
(50) Rossini, F. D.; Pitzer, K. S.; Arnett, R. L.; Braun, R. M.; Pimentel, G. C. *Selected Values of Physical and Themodynamic Properties of Hydrocarbons and Related Compounds*; Carnegie Press: Pittsburgh, 1953.
(51) Liu, X. Y.; Benemma, P. *J. Chem. Phys.* **1992**, *97*, 3600.
(52) Yamamoto, T. *J. Chem. Soc., Faraday Trans.* **1995**, *91*, 2559.
(53) Kraack, H.; Deutsch, M.; Sirota, E. B. Manuscript in preparation.
(54) Broadhurst, M. G. *J. Res. Natl. Bur. Stand.* **1966**, *70A*, 481.
(55) Hoffman, J. D.; Lauritzen, J. I.; Passaglia, E.; Ross, G. S.; Frolen, L. J.; Weeks, J. J. *Kolloid Z. Z. Polym.* **1969**, *231*, 564.
(56) Ungar, G. *Macromolecules* **1986**, *19*, 1317.
(57) Leute, U.; Dolhopf, W. *Colloid Polym. Sci.* **1980**, *258*, 353.
(58) Dorset, D. L. *Acta Crystallogr.* **1995**, *30*, 1021.
(59) Dorset, D. L. *J. Phys. D* **1997**, *30*, 451.
(60) Zhang, W. P.; Dorset, D. L. *J. Polym. Sci., Part B* **1990**, *28*, 1223.
(61) Dorset, D. L. *Macromolecules* **1999**, *32*, 162.
(62) Hermann, K.; Gerngross, O.; Abitz, W. *Z. Phys. Chem. (Munich)* **1930**, *B10*, 371.
(63) Flory, P. J. *J. Am. Chem. Soc.* **1962**, *84*, 2857.
(64) Lauritzen, J. I.; DiMarzio, E. A. *J. Res. Natl. Bur. Stand.* **1978**, *83*, 381.
(65) Guttman, C. M.; DiMarzio, E. A.; Hoffman, J. D. *J. Res. Natl. Bur. Stand.* **1980**, *85*, 273.
(66) While the fact that the density of the crystal and liquid are different would not geometrically permit such a nucleus of infinite lateral extent, Flory[63] pointed out that this is not a problem for a critical nucleus having small lateral dimension.
(67) Yamamoto, T. *J. Macromol. Sci., Phys.* **1979**, *B16*, 487.
(68) Langen, M. d.; Luigjes, H.; Prins, K. O. *Polymer* **2000**, *41*, 1193.
(69) Toner, J. *Phys. Rev. A* **1983**, *27*, 1157.
(70) Strey, H. H.; Wang, J.; Podgornik, R.; Rupprecht, A.; Yu, L.; Parsegian, V. A.; Sirota, E. B. *Phys. Rev. Lett.* **2000**, *84*, 3105.
(71) While there have been some quite detailed characterizations of the high-pressure hexagonal phase,[43,56,67,68] there are really some important open questions regarding its structure: Is the structure indeed a 2-dimensional hexagonal crystal? Is the correlation length infinite along the molecular (*c*-) axis? Or is it a line hexatic?[69,70] Does the nature or magnitude of this order vary over the $T-P$ range of the phase? Another characteristic, which while not determining the symmetry of the phase might be coupled to it, is: how an individual chain follows that structure. This is the degree that a given chain wanders laterally in the 2D lattice as it progresses along its length. Is this horizontal displacement confined within a single lattice spacing? Is it bounded? Or does it diverge, and if so, is it power-law or weakly logarithmic?
(72) Flory, P. J. *Statistical Mechanics of Chain Molecules*; Wiley: New York, 1969.

MA000312M